Density functional periodic study of CO adsorption on the $Pd_3Mn(100)$ alloy surface: Comparison with Pd(100)

F. Delbecq* and P. Sautet
Institut de Recherches sur la Catalyse, 2 Avenue Albert Einstein, 69626 Villeurbanne Cedex, France
and Ecole Normale Supérieure de Lyon, 46 allée d'Italie, 69364 Lyon Cedex 07, France
(Received 13 May 1998; revised manuscript received 26 October 1998)

Self-consistent calculations based on density-functional theory with gradient corrections are used to compare the electronic and chemisorptive properties of Pd(100) and $Pd_3Mn(100)$. There are two types of $Pd_3Mn(100)$ surfaces, one with only Pd atoms (*A*) and one with Pd and Mn atoms alternately ordered (*B*). The study of five-layer slabs shows that, for both surfaces, the surface Pd atoms are negatively charged by an electron transfer from the Mn atoms and that the ''giant'' magnetic moments existing on Mn atoms in the bulk are retained. For CO adsorption on $Pd_3Mn(100)$ (*A*), the adsorption sites are in the same stability order as for Pd(100), with the on-top site less stable than the bridge and the hollow ones while the binding energies are slightly weaker. In the case of $Pd_3Mn(100)$ (*B*), the stability order is totally different, with the on-top site on Pd far more stable than the other sites. It is pointed out that CO adsorption on a magnetic atom is less favorable than on a nonmagnetic one, in relation with an adsorption-induced diminution of the magnetic moment. The results are interpreted in terms of orbital interactions. [S0163-1829(99)03308-1]

I. INTRODUCTION

The electronic, chemical, and catalytic properties of metal-alloy surfaces have been extensively studied in a recent past. The reason is that metal alloys exhibit enhanced catalytic properties compared to those of their constituents, for instance a better activity and/or a better selectivity. It has been observed that in most cases, the adsorption energies of molecules on a metal surface are reduced when the metal is alloyed with another one. Carbon monoxide (CO) has often been used as a probe molecule for bringing to the fore such changes. The following experimental examples of CO adsorption on alloys can be quoted: on Pt/Sn,[1,2] on Ni/Sn,[3] on Pd/Sn,[4] on Pt/Fe,[5] on Pd/Cu,[6–8] and on Pd/Ni.[9] A theoretical understanding of how the properties of a metal are modified when it is alloyed is important for catalysis since it can help to improve the catalyst for a given reaction.

Most theoretical works deal with the electronic structure of thin films of a late transition metal deposited on an early one.[10–13] Adsorption of CO on such surfaces has also been studied theoretically.[14–16] To our knowledge, only a few theoretical studies deal with CO adsorption on real alloy surfaces: in Ref. 14 a calculation is done on Cu_3Pt (111) but without details. Adsorption on Pt_3Ti (111) and (100) surfaces has been more intensively studied with semiempirical methods.[17–18] Calculation for CO adsorption on pure metals are much more numerous.[19–25]

We have performed in the past semiempirical extended Hückel calculations (EHT) for CO adsorption on the $Pt_{80}Fe_{20}$ (111) and the Pd_3Mn alloy surfaces.[26–28] However to obtain a more quantitative description of the phenomenon, *ab initio* calculations must be envisaged. Hence, the purpose of this work is to use an *ab initio* method based on the density-functional theory (DFT) in order to compare the CO adsorption on Pd(100) and on $Pd_3Mn(100)$. The relation between surface magnetism and CO chemisorption will also be considered. The choice of this alloy comes from experimental studies performed in our laboratory where Pd/Cr and Pd/Mn alloys are used as efficient catalysts of the reduction of NO by CO.[29,30] Moreover, the Pd/Mn alloys have a more defined structure than Pd/Cr ones.

In a first part, the electronic structure of the surfaces will be studied. Then in a second part, the CO adsorption will be considered on the (100) surfaces of pure Pd and of the Pd_3Mn alloy.

II. METHODOLOGY

The method used is a self-consistent band calculation based on the density-functional theory in the Kohn-Sham approach (Programm ADF-BAND).[31] The one-electron wave functions are developed on a basis set of atomic orbitals. These basis functions are divided into a core part (numerical atomic orbitals NAO) and a valence part (NAO's plus Slater-type orbitals STO's) that is of double-ζ type. For the Pd atom, the core part includes orbitals up to the $3d$ ones. The starting configuration has been chosen to be $4d^9 5s^1$ in order to have a $5s$ NAO. This configuration improves the quality of the basis, but has no influence on the final solution, when the convergence is reached. A $5p$ STO has been introduced as a hybridization function. For the Mn atom, the core part includes orbitals up to the $2p$ one. The starting configuration is that of the ground state $3d^5 4s^2$. A $4p$ STO has also been added. For C and O, the $1s$ orbital has been frozen and $3d$ orbitals have been included as polarization functions. The $2s$ and $2p$ orbitals are represented by one NAO and two STO's (triple-ζ basis). The Slater exponents used in this work are as follows: Pd $4s$:3.85; $4p$:3.15; $4d$:1.5; $5s$:1.85; $5p$:1.85 $-$Mn $3s$:3.5; $3p$:3.0; $3d$:1.2; $4s$:2.0; $4p$:1.5$-$C $2s$:1.28 and 2.10; p:0.82 and 1.48; $3d$:2.2$-$O $2s$:1.72 and 2.88; $2p$:1.12 and 2.08; $3d$:2.0. The ADF code uses an auxiliary basis to fit the electronic density. A rather large set has been used: 60 STO's for Pd $(21s,13p,12d,8f,6g)$, 36 for Mn

$(15s,7p,6d,4f,4g)$, and 20 for C and O $(8s,5p,4d,2f,1g)$.

The wave function is calculated at the local density approximation level but gradient corrections for the exchange and the correlation energies are introduced (generalized gradient approximation, GGA), either from Becke–Perdew[32] or from Perdew-Wang.[33] Such gradient corrections proved to be essential in the determination of the chemisorption energies.[22,23] The calculations on Pd_3Mn are spin unrestricted since it has been shown experimentally and by our previous calculations[34] that the spin polarization is an essential feature for this alloy. The surfaces are modeled by slabs, infinite periodic in two dimensions x and y, and composed of a given number of layers in the z direction. Therefore, a single slab is considered and there is no periodicity in z. CO is adsorbed only on one side of the slab. The number of k-points depends on the symmetry of the adsorption site. This number is 15 for almost all sites except for the top site on $Pd_3Mn(A)$ and the hollow site on $Pd_3Mn(B)$ for which it is 25 (for definition of A and B see below). For the study of the bare surfaces, slabs of up to five layers have been considered. For the adsorption, slabs of only two and three layers have been used owing to the disk space required by the calculations. The lattice constant has been taken equal to that optimized for the bulk at the GGA level, which corresponds to a Pd-Pd distance of 2.85 Å for both systems.[34] The M-C and C-O bond lengths have been optimized for all adsorption sites on the two-layers slab with no inclusion of surface relaxation. The calculation of the electronic populations is based on a Mulliken analysis.

III. ELECTRONIC AND MAGNETIC STRUCTURES OF THE Pd(100) AND Pd_3Mn(100) SURFACES

The Pd_3Mn alloy presents interesting magnetic properties since a so called ''giant moment'' is present on each Mn atom. The question is therefore to know how this magnetic behavior evolves on the surface and whether the magnetic structure of the surface has an influence on the chemisorption. Theoretical calculations have predicted a large enhancement of the magnetic moment of $3d$ transition-metal surfaces compared to the bulk.[35–37] Most of the theoretical works in this area also deal with monolayer of transition metals deposited on a substrate. For the metals considered in this work (Pd, Mn) one can cite a full-potential linearized augmented-plane-wave (FLAPW) calculation of a Mn overlayer on Pd(100).[38] In a recent work, the magnetic nature of (100) surfaces of binary alloys has been studied.[39] In what concerns pure Pd(100), one can wonder whether Pd surfaces can be ferromagnetic since Pd has a strong magnetic susceptibility and since an abrupt paramagnetic-ferromagnetic phase transition occurs in bulk Pd for a 6% lattice expansion. Spin-polarized FLAPW calculations show that the ground state for Pd(111) and Pd(100) is nonmagnetic.[36,40] Nevertheless a monolayer of Pd(100) has been calculated to be ferromagnetic with a moment of 0.42 μB per atom.[41]

1. The Pd(100) surface

The electronic population and the magnetic moment of the surface atoms Pd(S), the second layer atoms Pd($S-1$) and the center-layer atoms Pd(C) for a five-layer slab of Pd(100) are given in Table I. The interesting fact is the existence of a magnetic moment on the Pd atoms whereas no magnetic moment had been found for bulk Pd with the same Pd-Pd distance.[34] This surface magnetic moment (0.14 μB) is smaller than that found for a monolayer,[41] which is not surprising since the surface Pd atoms are less isolated than in a monolayer. In fact, we have already pointed out that Pd has a high-magnetic susceptibility. It results that a small modification of the Pd-Pd interactions leads to the abrupt appearance of a magnetic moment.[41] It has been found that a moment appears when the lattice parameter is expanded, attains a maximum value (0.36 μB) and then falls continuously to zero. Our value of 0.32 μB found in the central layer is near this maximum value found previously for the bulk. In fact, calculations up to a slab of eleven layers have been done. A magnetic moment still exists on the surface (ca. 0.1 μB) and its value is 0.22 μB for the central layer. Therefore, the variations of the magnetic moment with the layer can be ascribed to small variations in the Pd atoms interactions.

TABLE I. Characteristics of Pd(100) and Pd_3Mn(100) five-layer slabs. S, S-1 and C denote a surface atom, a second-layer atom and a center-layer atom, respectively. q (e^-) and μ (μB) are the charge and the magnetic moment, respectively. In Pd_3Mn (A) the surface only contains Pd atoms. In Pd_3Mn (B) the surface contains both Pd and Mn atoms.

	Pd		Pd_3Mn (A)		Pd_3Mn (B)	
	q	μ	q	μ	q	μ
Pd(S)	0.02	0.14	−0.07	0.08	−0.23	0.11
Pd(S-1)	−0.02	0.27	−0.18	0.11	−0.17	0.08
Pd(C)	0	0.32	−0.16	0.09	−0.17	0.07
Pd bulk	0	0	−0.17	0.11	−0.17	0.11
Mn(S)					+0.41	4.56
Mn(S-1)			0.47	4.31		
Mn(C)					0.49	4.23
Mn bulk			0.51	4.29	0.51	4.29

The density of states curve (DOS) projected on a surface Pd atom of Pd(100) is given in Fig. 1. Due to a reduced coordination number at the surface (8 instead of 12), the d band of the surface Pd atoms is narrower compared with the bulk. The shape of the DOS begins to be very similar to that of the bulk when the central layer (C) is considered.

The value computed for the Fermi level is −5.35 eV in the case of the two-layer slab. The considered system is a single slab and the energy reference for the Fermi-level calculation is the vacuum level at an infinite distance from the slab. For the three-layer slab the value depends strongly on the screening of Coulomb potentials in lattice summations. The cutoff parameter must be large, which is restricted by the computation cost. For a very large cutoff parameter we found $E_F = -5.38$ eV, value close to that obtained for the two-layer slab. In the following, we will only give E_F for the latter. Experimental values of the work-function range between 5.3 and 5.8 eV (Refs. 42–45) and another calculation also gives 5.3 eV.[46]

2. The Pd_3Mn(100) surfaces

Pd_3Mn crystallizes in a disordered fcc structure (Cu_3Au type) above 800 K and in an ordered tetragonal one (Al_3Zr

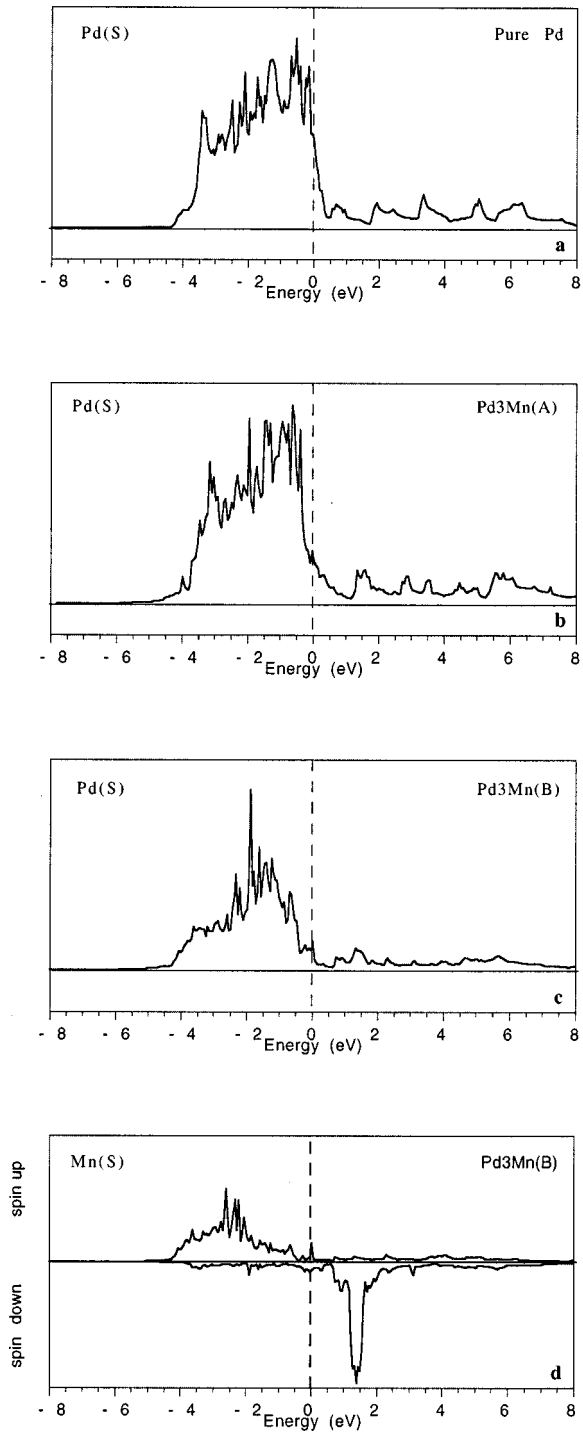

FIG. 1. DOS projected on a surface Pd atom for a five-layer slab of Pd(100) (a), $Pd_3Mn(100)$ *A* (b) and $Pd_3Mn(100)$ *B* (c) and DOS projected on a surface Mn atom for $Pd_3Mn(100)$ *B* (d).

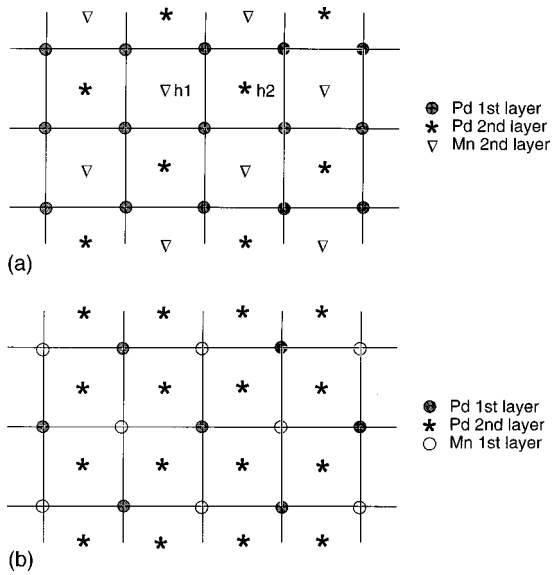

FIG. 2. Two-layer slab models of $Pd_3Mn(100)$ with only Pd atoms in (a) the surface layer (*A*) and with both Pd and Mn atoms in (b) the surface layer (*B*).

type) below this temperature.[47,48] In the latter structure Cu_3Au-type unit cells are separated by antiphase domain boundaries resulting in a unit cell four times greater (16 atoms). For a question of size we have chosen to consider here the single fcc unit cell of Cu_3Au type, which retains the basic properties of the alloy. The (100) planes of such an alloy either contain only Pd atoms or contain a mixture of Pd and Mn atoms in equal quantities. These two types of planes alternate and the surface of the resulting slabs can be of either type. Therefore, there are two types of (100) surface that are represented on Fig. 2.

Let us consider first a five-layer slab of $Pd_3Mn(100)$ with a surface containing only Pd atoms (type *A*). Like for the Pd(100) slab, the electronic populations q and the magnetic moments μ of the various atoms are given in Table I. One observes that for Pd (*S*) (at the surface) q is smaller than that of the atoms of the other layers, which is close to the value found for the bulk. Nevertheless, the electronic transfer from Mn to Pd that exists in the bulk remains and the Pd surface atoms in $Pd_3Mn(100)$ are more negatively charged than in the case of pure Pd (-0.07 vs $+0.02$). Both the *d* and the *sp* orbitals gain electrons (0.05 and 0.04, respectively). Our system could be considered as a Pd overlayer deposited on a four-layer slab of Pd_3Mn. There is a controversy in the electronic structure of metal atoms like Pd deposited on a more electropositive metal: the experimental data show that the binding energy of the Pd $3d_{5/2}$ state is increased compared with that on pure Pd. This fact has been interpreted by a charge transfer from Pd to the more electropositive metal in opposite to the situation found in the bulk.[49] However, other explanations have also been given, like the strength of the bond between the two metals,[50] the changes in reference level and hybridization[51] or a charge transfer towards the interface region.[52] Our results based on a Mulliken analysis tends to show that the electron transfer at the type *A* surface of the Pd_3Mn alloy is in the same direction as in the bulk and follows the electronegativity difference between the two metals.

Concerning the magnetic moment μ, one observes that it does not vary much with the layer and is very close to the bulk value. The interesting fact is that the magnetic moment on Pd is smaller than in the slab of pure Pd (for instance 0.11 vs 0.32 μB for the central layer). Concerning the Mn atoms of the second layer, μ is large and very similar to its value in the bulk (4.31 vs 4.29 μB).

Compared to the DOS projected on Pd(*S*) for Pd(100), the DOS projected on Pd(*S*) for $Pd_3Mn(100)$, type *A* is nar-

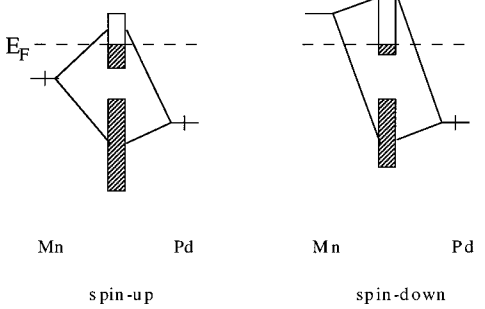

FIG. 3. Schematic interaction diagram of the spin-up and spin-down *d* orbitals of Pd and Mn atoms.

rower and farther from the Fermi level [Figs. 1(a) and 1(b)]. This results from the fact that the interactions between atoms of different metals are weaker than the interactions between atoms of the same metal. One observes a small peak at 1.5 eV corresponding to the antibonding interaction with the Mn orbitals, which are higher in energy.

Let us consider now a five-layer slab of $Pd_3Mn(100)$ with a surface containing both Pd and Mn atoms (type *B*). The Pd surface atoms are more negatively charged than for the surface of type *A* and than in the bulk. Compared with surface Pd atoms of pure Pd, the *d* orbitals gain $0.10e^-$ and the *sp* orbitals gain $0.15e^-$. Therefore, our Mulliken analysis shows that the electron transfer towards a Pd atom of a type *B* surface of $Pd_3Mn(100)$ follows the electronegativity scale and is even larger than in the bulk.

The Pd magnetic moment does not vary significantly with the layer. However, the magnetic moment of a Mn surface atom is larger than in the bulk (4.56 vs 4.29 μB) in agreement with the literature.[35–37,53] This can be explained by considering the orbital interactions of Fig. 3. The spin-up orbitals of both Mn and Pd atoms are full ($5e^-$). Their interaction leads to an antibonding band concentrated on Mn, the position of which relative to E_F depends on the strength of the interaction. On the surface compared with the bulk, the coordination is smaller and the interaction weaker. The antibonding band is less pushed above E_F and is therefore more occupied [$4.94e^-$ vs $4.87e^-$ (Ref. 34)]. The spin-down orbital of a Mn atom is empty. By interaction with the full spin-down orbital of Pd the bonding combination can be pushed below E_F and hence the spin-down band gains electrons. This gain also depends on the strength of the interaction. On the surface compared to the bulk, the weaker interaction leads to a smaller part of the upper band being pushed below E_F and hence, to a smaller occupation of the Mn spin-down band [0.53 vs $0.66e^-$ (Ref. 34)]. Therefore on the surface, the Mn spin-up band is more occupied and the Mn spin-down band less occupied. This leads to an enhanced magnetic moment. The *sp* band also contributes to the magnetic moment but to a smaller extent.

The DOS projected on a Pd surface atom looks very different from that obtained for the pure Pd(100) surface or the type-*A* $Pd_3Mn(100)$ surface [Fig. 1(c)]. It is much narrower and farther from E_F. This is due to the decreasing number of neighboring Pd atoms and the concomitant increasing number of neighboring Mn atoms when going from pure Pd to surface *A* and surface *B* (8Pd, 0Mn; 6Pd, 2Mn and 4Pd, 4Mn, respectively). The DOS projected on each spin for a Mn surface atom is also given [Fig. 1(d)].

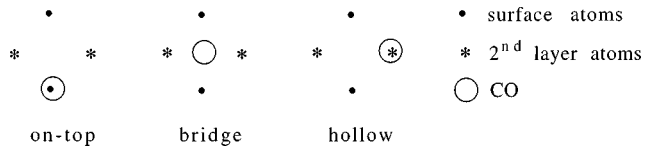

FIG. 4. Representation of the three studied adsorption sites.

The Fermi level E_F has been determined for the two-layer slab. A value of -4.94 eV has been found. Compared to -5.35 eV found for Pd(100), the Fermi level has been raised by 0.4 eV by the alloying with Mn, which is more electropositive than Pd.

In conclusion to the study of the electronic properties of the $Pd_3Mn(100)$ alloy surfaces compared with the Pd(100) surface, the important changes in the electronic occupations and in the DOS shapes of the Pd surface atoms have been underlined. The existence of atoms (Mn) with a large magnetic moment has also been pointed out in the case of the type-*B* $Pd_3Mn(100)$ surface. We will now see how these changes influence the adsorption ability of the Pd atoms towards CO.

IV. CO ADSORPTION

The adsorption of CO on Pd(100) is well experimentally documented.[54–60] Bridge CO has only been detected and the low-energy electron diffraction LEED analysis led to 1.15 and 1.93 Å for the C-O and Pd-C bond lengths, respectively.[55,56] Nevertheless, a partial occupation of fourfold sites at low coverage has been postulated.[56] A binding energy of 36 kcal/mol has been extrapolated at zero coverage[54] with a decrease of 8 kcal/mol at a coverage $\theta = 0.5$. Another determination gives $E_{ad} = 38.5$ kcal/mol up to a coverage of $\theta = 0.45$ and $E_{ad} = 26$ kcal/mol at $\theta = 0.6$.[56] At $\theta = 0.5$ the real structure is $c(2\sqrt{2}\times\sqrt{2})R45°$ with two CO molecules in the unit cell.

Only a few data exist concerning the adsorption of CO on Mn. It seems that CO adsorbs in both the dissociative and the molecular forms.[61] The heat of adsorption on polycrystalline surfaces have been measured for Mn (78 kcal/mol) and Pd (43 kcal/mol).[62]

1. Adsorption on Pd(100)

The three possible adsorption sites have been considered, on-top, bridge and fourfold hollow (Fig. 4). The unit cell is composed of two Pd atoms and one CO molecule per layer, which leads to a coverage of $\theta = 0.5$ and a $c(2\times2)$ structure, which is less stable than the experimental one owing to slightly stronger repulsions between the CO molecules.[56] Our choice is imposed by the size of the calculations. The Pd-C and the C-O bond lengths have been optimized on the two-layer slab. Nevertheless, it has been verified that the Pd-C bond optimization with the three-layer slab gives the same result for the bridge site (2.06 Å). A fragmentation of the whole system in two parts, the metal slab and the CO molecule, has allowed us to obtain the electronic populations of the CO molecular orbitals (3σ, 4σ, 1π, 5σ, 2π). The binding energies (BE) are defined as the difference between the

TABLE II. CO adsorption on a three-layer slab of Pd(100). Optimized bond lengths Pd-C and C-O (in Å), binding energies BE (in kcal/mol), overlap population op, electron loss (−) or gain (+) of the CO molecular orbitals.

	Top	Bridge	Hollow
Pd-C[a]	1.91	2.05	2.28
C-O[a]	1.15	1.16	1.18
BE (BP)[b]	−25.4	−30.2	−32.5
BE (PW)	−28.5	−33.4	−36.4
C-O op	0.619	0.591	0.504
Pd-C op	0.335	0.420	0.514
Pd-Pd op (0.327)[c]	0.272	0.206	0.189
loss of 5σ	−0.46	−0.50	−0.47
gain of $2\pi_x$	0.21	0.20	0.33
gain of $2\pi_y$	0.21	0.27	0.33

[a]The geometry optimizations are done for the two-layer slab.
[b]BP: Becke 88-Perdew 86; PW=Perdew/Wang 91. See text.
[c]op between the two Pd surface atoms shown in Fig. 4. In parenthesis, values for the bare slab.

energy of the whole system and the energies of each interacting part, the bare slab and gas phase CO. A negative value means a stabilizing interaction. All the results for adsorption on the three-layer slab, with the geometries obtained for the two-layer one, are given in Table II. The two values of BE correspond to two different gradient corrections, either BP (Becke 88 and Perdew 86) or PW (Perdew-Wang 91).

Let us comment on these results. The optimized bond lengths for the bridge site are slightly larger than the experimental one (2.05 vs 1.95 and 1.16 vs 1.15 Å). Following the experimental trends for surfaces and complexes, the Pd-C bond length increases from the top to the hollow site [see Refs. in 19]. Connected to a decrease in the C-O overlap population, we observe an increase of the C-O bond length. This is in agreement with the experimental decrease of ν_{CO} from the top to the hollow site.

Concerning the binding energies, several comments can be made. First, the PW functional gives BE higher by ca 3 kcal/mol than the BP one but the relative order of the various sites is preserved. Secondly, the hollow site is slightly more stable than the bridge one by 2 kcal/mol. This difference is not significant but leads nevertheless to the conclusion that the hollow and the bridge sites are close in energy. This result confirms that occupation of fourfold sites at low coverage can be postulated.[56] This energy order between sites is not modified if the experimental Pd-Pd distance is used in the slab instead of the calculated optimal value of 2.85 Å. The on-top site is far less stable. To evaluate the effect of the coverage on the binding energy, we performed a calculation on a $p(2\times2)$ bridge structure (four Pd atoms and one CO per unit cell, $\theta=0.25$, two layers). We found −35.9 and −39.1 kcal/mol for the BP and PW binding energies, respectively, which represents a gain of 3 kcal/mol relative to the values at $\theta=0.5$ for the two-layer slab (−32.8 and −36.1 kcal/mol, respectively). Our values are in the range of the experimental ones. How can the binding energies be related to the variations of the overlap populations (op)? From the on-top to the bridge and the hollow sites, the Pd-C op increases, which reflects a better interaction of CO with the surface. However, at the same time, the Pd-Pd op between the surface atoms decreases, which means a loss of surface stability. These two effects are opposite and the resulting binding energy is a compromise. This fact has already been pointed out.[19] The variation of Pd-Pd op during adsorption explains the surface reconstruction observed experimentally but that we have not considered here.

Since a small magnetic moment exists on the Pd surface atoms, we have also performed calculations with spin polarization for the bridge and the hollow sites. No significant effect is observed, the BE variation being 0.1 kcal/mol.

The Fermi level is calculated to be −5.9, −6.2, and −6.6 eV for the on-top, bridge and hollow sites, respectively, which yields an increase of the work function of 0.55, 0.85, and 1.25 eV [E_F for Pd(100) being −5.35 eV]. The work function change $\Delta\Phi$ induced by CO adsorption on the bridge site has been measured experimentally.[56,63,64] The value varies in a rather large range from 0.8 eV (Ref. 63) to 0.93 eV (Ref. 56). But it has been shown that $\Delta\Phi$ depends strongly on the presence of carbon impurities and on the coverage. A value of 0.7 eV has been assumed in Ref. 44 with a work-function value for Pd(100) at 5.8 eV. The $\Delta\Phi$ value calculated in the present work for the bridge site falls in this range.

The interaction of CO with the surface can be expressed in terms of molecular-orbital interaction as it has been already pointed out in the Blyholder model.[65] Our fragmentation procedure allows us to obtain the variations of the electronic population of the various CO orbitals (Table II). For the three adsorption sites, the contributions of the 3σ and 4σ orbitals are very negligible (not given in the table), as are also those of the 1π orbitals. The main electronic transfers occur from the 5σ and toward the 2π orbitals, in agreement with the Blyholder model. By interaction with 5σ some d states are destabilized and pushed above E_F. Inversely the interaction with 2π stabilizes them and pushed them below E_F. This interaction is qualitatively described in Fig. 8 (left). It explains why 5σ loses electrons since the antibonding states above E_F have some 5σ character and why 2π gain electrons since the bonding states below E_F have some 2π character. The donation from 5σ does not vary much from the on-top site, to the bridge and the hollow ones. In contrast the back donation to the 2π orbitals increases, especially for the hollow site. Our calculations verify the relation between the increase of the back-donation and the increase of the work-function change ($\Delta\Phi$), as it has been postulated previously[64] (see above).

From the calculation of projected DOS it can be seen that, after interaction with the surface, 5σ and $1\pi_y$ give a peak at the same energy (−6.1 eV below E_F), 5σ being more efficiently stabilized. The peaks associated with 4σ and $1\pi_x$ are −8.6 and −5.6 eV below E_F, respectively. The 2π orbitals have contributions below E_F and their main associated peak above E_F is broad (ca. 3 eV), which means that they mix strongly with the metal-d orbitals.

The inverse photoelectron spectroscopy is a technique capable of probing the unoccupied levels of a molecule adsorbed on a surface. The ultraviolet photoelectron spectroscopy leads on the contrary to the positions of the occupied orbitals of adsorbates. Such experiments done for CO on Pd(100) show that 2π gives a large peak (ca. 2-eV broad)

TABLE III. CO adsorption on a three-layer slab of $Pd_3Mn(100)$ type *A* (only Pd atoms in the surface). Optimized bond lengths Pd-C and C-O (in Å), binding energies BE (in kcal/mol), overlap population op, electron loss (−) or gain (+) of the CO molecular orbitals, magnetic moment μ (in μB).

	Top	Bridge	Hollow 1	Hollow 2
Pd-C[a]	1.92	2.07	2.29	2.29
C-O[a]	1.15	1.16	1.18	1.18
BE (BP)[b]	−19.7	−26.8	−21.9	−32.5
BE (PW)	−22.9	−30.2	−25.8	−36.4
C-O op	0.615	0.584	0.516	0.502
Pd-C op	0.327	0.426	0.494	0.506
Pd-Pd op (0.329)[c]	0.279	0.218	0.210	0.191
loss of 5σ[d]	−0.44	−0.47	−0.46	−0.46
gain of $2\pi_x$	0.20	0.21	0.32	0.35
gain of $2\pi_y$	0.20	0.29	0.32	0.35
μCO	0	0.01	−0.03	0.03
μ Pd (0.07)[e]	0.02	0.05	−0.01	0.06
μ Mn (4.33)[e]	4.31	4.36	4.27	4.39

[a]The geometry optimizations are done for the two-layer slab.
[b]BP: Becke 88-Perdew 86; PW=Perdew/Wang 91. See text.
[c]op between the two Pd surface atoms shown in Fig. 4. In parenthesis, values for the bare slab.
[d]The population analysis is given for the geometries optimized on Pd(100).
[e]Values for the bare slab.

centered at 4.8 eV above the Fermi level[44] and that the $5\sigma+1\pi$ level and the 4σ level are located at −7.9 and −10.8 eV, respectively, below the Fermi level.[56,66] Although the DFT one-electron energies have no connection to the experimental excitation spectrum and therefore the absolute values are not reliable, the calculated broadening of the 2π peak and the energy difference between 4σ and $5\sigma+1\pi$ peaks are in reasonable agreement with the experimental data.

The conclusion of this study of CO adsorption on Pd(100) is that our results reproduce well the experimental data. The advantage of the method used is that it allows the interpretation of the results by means of molecular orbital interactions. We have seen in Sec. III-2 that the metal orbitals are modified by alloying. We will, therefore, investigate in the next section what changes are introduced by these modifications when CO is adsorbed on Pd_3Mn. We will consider successively the two types of $Pd_3Mn(100)$ surfaces.

2. Adsorption on $Pd_3Mn(100)$ type *A*

The same adsorption sites have been studied, on-top, bridge, and hollow. On this surface where only Pd atoms are present in the first layer, two different hollow sites can be found depending on the presence of a Mn atom (hollow 1) or of a Pd atom (hollow 2) just below in the second layer (see Fig. 2). The results are given in Table III. As previously, the Pd-C and C-O bond lengths have been optimized for the two-layer slab. The optimized geometries do not differ much from those found on Pd(100) (compare Tables III and II) and the variation of the electronic population of the CO orbitals is given for the geometries found on Pd(100) in order to compare the effects at equal distances.

Let us comment on Table III. The same observation as before can be done concerning the variation of the bond lengths, of the overlap populations and of the binding energies when the various sites are compared. The hollow 2 site [that is the same as on Pd(100) with a Pd atom below it] is also the most stable. The hollow 1 site is significantly less stable. If one considers the losses and gains of CO orbitals, the variation are weak between the two hollow sites: same 5σ donation and small increase in the back donation into 2π. This means that the stabilizing two-electrons interactions are only slightly stronger for the hollow 2 site, which is reflected by a slightly larger Pd-C overlap population. In our work with the extended Hückel method,[28] we have pointed out the important role of the destabilizing four-electron interactions for explaining the relative order of the binding energies. If we look here at the negative atomic overlap populations that represent repulsions, we observe that the C atom has a negative overlap population with the atom just below it in the second layer, which is only 3.08 Å away (op=−0.03 with Pd and −0.05 with Mn). Hence, the repulsion is slightly stronger for the hollow 1 site, which also tends to favor the hollow 2 site.

Let us now compare the adsorption on Pd_3Mn (*A*) with that on Pd(100). First one observes a slight decrease in the binding energies except for the hollow 2 site. In all cases, the donation from 5σ is decreased for the alloy compared to the pure metal. The variation is not as clear for the back donation into 2π since it decreases for the on-top site and increases for the hollow 2 site.

The CO overlap population does not vary much either except a small diminution for the bridge site. The work-function change $\Delta\Phi$ is smaller than for Pd(100):0.44, 0.54, and 0.77 eV for the on-top, the bridge and the hollow site, respectively.

Concerning the magnetic behavior of the $Pd_3Mn(100)$ surface of type *A*, one observes that a small magnetic moment μ appears on CO in the case of the hollow sites. However, its value is not significant. The small moment of Pd remains roughly the same and that of Mn in the second layer is not significantly affected by CO adsorption.

The changes in CO adsorption induced by alloying are therefore small in the case of surface of type *A* where only Pd atoms are present at the surface and their interpretation in terms of orbital interactions or DOS shapes is difficult. We will see in the next section that the changes are more important for the surface of type *B* and we will give the interpretations for this case. Nevertheless, the main conclusion to the study of surface *A* is the small decrease of the binding energy relative to that obtained on pure Pd.

3. Adsorption on $Pd_3Mn(100)$ type *B*

On this surface there are two on-top sites, one on a Pd atom and one on a Mn atom. There is only one bridge site involving a Pd and Mn atoms and one hollow site between two Pd and two Mn atoms and above a Pd atom in the second layer (see Fig. 2). In the CO adsorption study on Pt_3Ti, it has been suggested that CO can lie parallel to the surface, with the oxygen atom pointing towards Ti.[67] Since Mn atoms are present in the Pd_3Mn surface type *B*, such parallel geometries involving Mn have been investigated. In

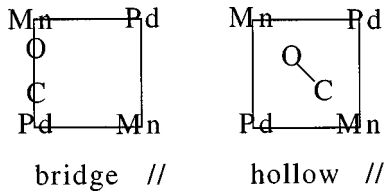

FIG. 5. Geometries of CO adsorption modes parallel to the surface.

order to optimize them more easily, we used another program, which allows conjugate gradient optimization. This is the VASP program (Vienna *ab initio* package simulation) which performs *ab initio* quantum-mechanical molecular dynamics using pseudopotentials and a plane-wave basis set.[68] In the first geometry considered, called bridge ∥, CO lies between a Pd and a Mn atoms parallel to the PdMn direction (Fig. 5). This geometry is not stable and evolves during the optimization into a geometry, which is similar to the on-top one. In the second geometry, called hollow ∥, CO lies along the diagonal of a lattice square. A stable structure is found with the following bond lengths: Pd-C=2.26 Å, Mn-C =2.07 Å, Mn-O=2.44 Å, and C-O=1.22 Å. The latter value is similar to that found for aldehydes and ketones. Nevertheless, this structure is less stable than the on-top one by 0.4 eV and will not be considered further. Therefore, CO adsorption parallel to the surface is not favorable on the Pd_3Mn alloy. With the program VASP, we also optimized the bridge site in order to find the relation between the Pd-C and Mn-C bond lengths. We found Mn-C longer than Pd-C by 0.15 Å. Then we reoptimized this site with ADF-BAND by keeping this difference constant.

The results for the four classical geometries described at the beginning of this section are given in Table IV. Contrary to what happens on Pd(100) and $Pd_3Mn(100)$ type *A* surfaces, the most stable adsorption site is the on-top one on a Pd atom and the hollow site is far less stable. In fact, it appears that the sites involving a Mn atom are unfavorable. This means that, if on the two former surfaces the bridge and hollow sites are more populated at low coverage, on Pd_3Mn type *B* the Pd on-top site must be more populated.

The CO overlap population is slightly decreased compared to the previous cases, which means that the CO bond is a little weaker on the surface of type *B*. The donation of the 5σ orbital is slightly decreased compared with the case of Pd(100) and varies very little relative to $Pd_3Mn(100)$ type *A*. On the contrary, the back donation into 2π, which does not vary much for the surface of type *A* compared to Pd(100) is significantly increased for the surface of type *B*. This explains the larger diminution of the C-O overlap population.

Concerning the magnetic behavior, we observe that the small magnetic moment of Pd is decreased except for the on-top adsorption on Mn. More interesting is the variation of μ on Mn. This moment diminishes slightly for the top site on Pd but largely when Mn is involved in the adsorption site: -0.73, -0.34, and -0.50 μB for the top on Mn, bridge and hollow sites, respectively.

Let us now consider the DOS projected on the various orbitals of the surface atoms. We chose to study d_{z^2} and d_{xz} (d_{yz}) which stick out of the surface and are the most involved in the adsorption. In Fig. 6 are drawn the DOS projected on Pd orbitals for Pd(100) on the left and on $Pd_3Mn(100)$ *B* on the right. In Sec. III, the total DOS projected on Pd surface atoms on both surfaces have been compared. The same conclusions are found here: the DOS projected on d_{z^2} and d_{xz} (d_{yz}) are narrower (especially d_{z^2}) and farther from the Fermi level on Pd_3Mn compared to Pd. For d_{xz} (d_{yz}) one observes small peaks above E_F corresponding to the antibonding combination with Mn orbitals (Fig. 6c′).

For the on-top adsorption sites, the main interactions occur between 5σ and the d_{z^2} metal orbital and between $1\pi_x$ and $2\pi_x$ and the d_{xz} metal orbital (or $1\pi_y-2\pi_y$ and d_{yz}) following Fig. 7. These interactions are depicted in Figs. 6(b), 6(b′) and 6(d), 6(d′) for the adsorption on a Pd atom. Part of the antibonding interaction between 5σ and d_{z^2} is pushed above E_F (Fig. 8). On the alloy surface, d_{z^2} being farther below E_F can less easily be pushed above it (Fig. 8 right) and loses less electrons than on pure Pd (-0.22 vs -0.34), which leads to a less stabilizing interaction since such states are metal-adsorbate antibonding. The smaller interaction is also reflected by the smaller loss of 5σ. The d_{xz} orbital interacts both with $1\pi_x$ and $2\pi_x$ [Figs. 6(d), 6(d′)]. Following Fig. 8, the interaction with $1\pi_x$ tends to shift it up and the interaction with $2\pi_x$ tends to shift it down. In the case considered here, the d_{xz} orbital (or *dyz*) loses more electrons for the Pd_3Mn alloy than for the pure metal (-0.08 vs -0.03), which means that the interaction of d_{xz} (d_{yz}) with the π_x (π_y) system is stronger. Besides, $2\pi_x$ ($2\pi_y$) gains more electron in the alloy case (0.25 vs 0.21). Effectively, the Fermi level being higher for the alloy, the $2\pi_x$ ($2\pi_y$)

TABLE IV. CO adsorption on a three-layer slab of $Pd_3Mn(100)$ type *B* (Pd and Mn atoms in the surface). Optimized bond lengths Pd-C, Mn-C, and C-O (in Å), binding energies BE (in kcal/mol), overlap population op, electron loss (−) or gain (+) of the CO molecular orbitals, magnetic moment μ (in μB).

	Top Pd	Top Mn	Bridge	Hollow
Pd-C[a]	1.92		2.05	2.37
Mn-C[a]		2.01	2.20	2.37
C-O	1.15	1.15	1.17	1.18
BE (BP)[b]	−24.3	−15.4	−20.4	−17.8
BE (PW)	−27.7	−18.9	−24.0	−21.8
C-O op	0.596	0.591	0.563	0.495
Pd-C op	0.354		0.257	0.271
Mn-C op		0.306	0.195	0.236
Pd-Mn op (0.422)[c]	0.331	0.318	0.255	0.260
loss of 5σ[d]	−0.44	−0.44	−0.46	−0.44
gain of $2\pi_x$	0.25	0.23	0.25	0.39
gain of $2\pi_y$	0.25	0.23	0.34	0.39
μ CO	−0.02	−0.08	−0.03	−0.01
μ Pd (0.14)[e]	0.01	0.19	0.06	0.09
μ Mn (4.56)[e]	4.50	3.92	4.25	4.20

[a]The geometry optimizations are done for the two-layer slab.
[b]BP: Becke 88-Perdew 86; PW=Perdew/Wang 91. See text.
[c]op between the Pd and Mn surface atoms shown in Fig. 4. In parenthesis, values for the bare slab.
[d]The population analysis is given for the geometries optimized on Pd(100).
[e]Values for the bare slab.

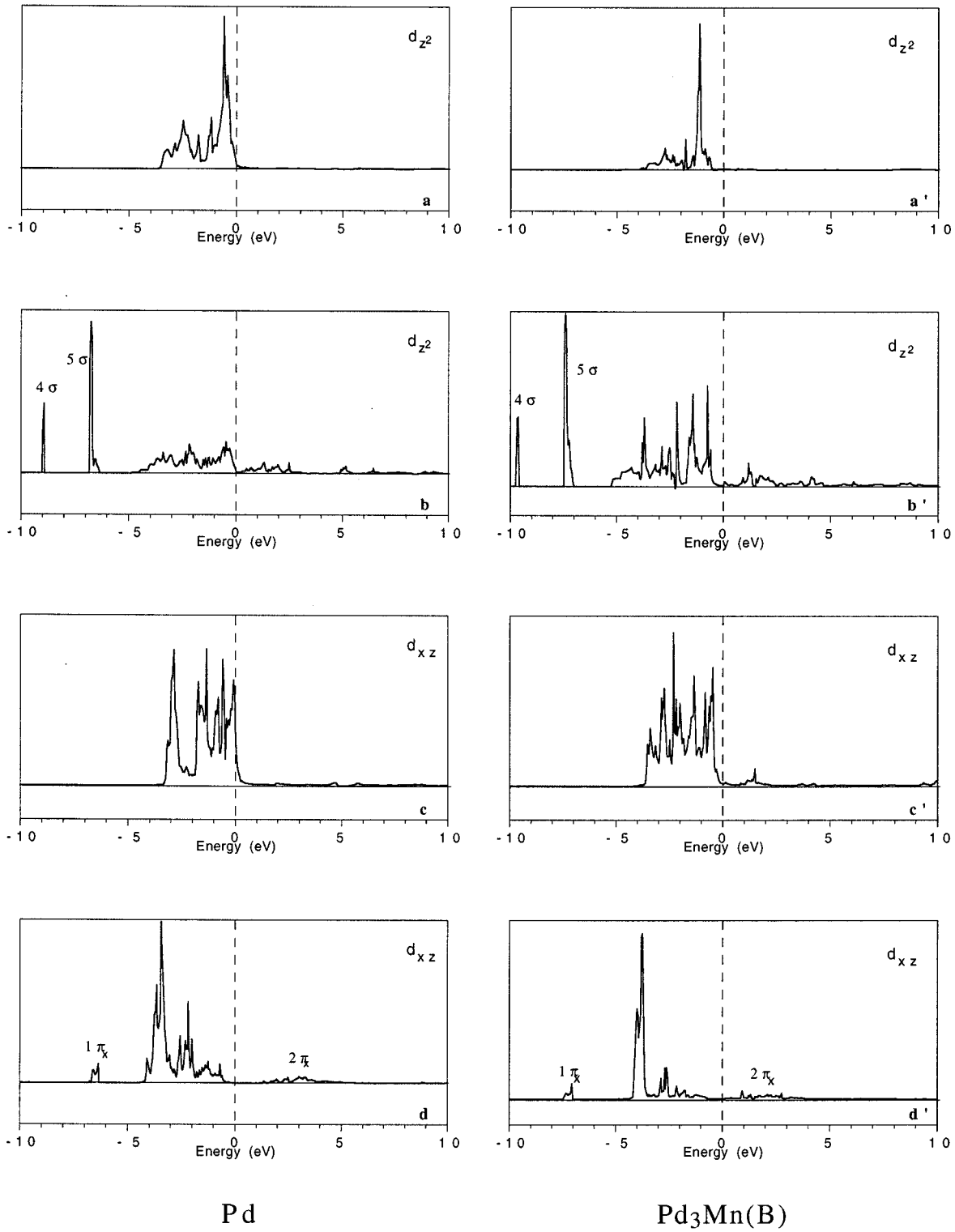

FIG. 6. DOS projected on d_{z^2} and d_{xz} of a Pd surface atom for the bare Pd(100) slab (a) and (c) and for the bare Pd_3Mn *B* slab (a′) (c′)—DOS projected on the same orbitals for the CO adsorption on-top on Pd for Pd(100) (b) and (d) and for Pd_3Mn *B* (b′) (d′).

orbital of CO in the gas phase is closer to it and therefore the bonding part of its interaction with the metal has a larger contribution below E_F (Fig. 8 right). The better interaction of the 2π orbitals prevails over the smaller interaction of the 5σ orbital and the interaction of CO in the top on Pd site is overall better for the alloy than for pure Pd. Accordingly, the Pd-C overlap population is greater on the alloy (0.359) than on Pd (0.336). Moreover, the overlap population with the first neighbors in the surface layer is larger for the alloy (op Mn-C=0.09) than for Pd (op Pd-C=0.05) which reflects a supplementary better interaction between CO and the alloy surface for the Pd on-top site.

Let us study now the on-top adsorption on a Mn atom. The DOS projected on d_{z^2} and d_{xz} for this Mn atom are given in Fig. 9 for the bare Pd_3Mn (*B*) surface (*a*,*c*) and for the on-top Mn adsorption (*b*,*d*). One observes a large broad-

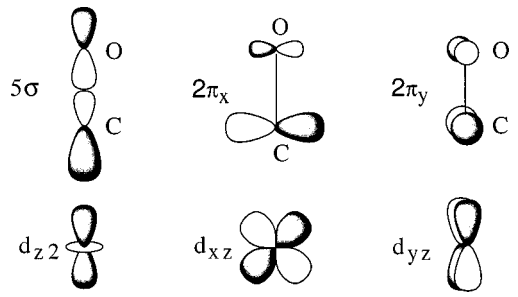

FIG. 7. Main interactions between the CO molecular orbitals and the metal orbitals in the on-top site.

ening of the bands after adsorption, especially for the d_{z^2} band. The Mulliken population analysis shows that these orbitals gain electrons instead of losing electrons as it was the case for the on-top adsorption on Pd ($+0.043$ for d_{z^2} and $+0.065$ for d_{xz} or d_{yz}). This comes from the fact that the Mn orbitals are partially empty. Let us consider the DOS projected on d_{z^2} [Figs. 9(a) and 9(b)]. For the bare surface the spin-up band is full ($0.99e^-$) and the spin-down band is almost empty ($0.08e^-$). The interaction of the spin-up band with the spin-up 5σ orbital is of the same kind as previously and shifts up this band above E_F, leading to a loss of electrons ($-0.117e^-$). However, the interaction of the full 5σ spin-down orbital with the empty spin-down d_{z^2} orbitals leads to a partial filling of the latter ($+0.160e^-$). The result is that d_{z^2} globally gains electrons and that its associated magnetic moment decreases from 0.91 to 0.64 μB.

Let us consider now the interaction of d_{xz} (d_{yz}) with $1\pi_x$ and $2\pi_x$ ($1\pi_y$ and $2\pi_y$) [Figs. 9(c) and 9(d)]. The spin-up d_{xz} band, which is almost full for the bare surface ($0.99e^-$), loses electrons (-0.06) since a small part of it takes part to the antibonding interaction with $2\pi_x$ above E_F and the spin-up part of $2\pi_x$ gains electrons (0.105). The spin-down d_{xz} band, which is empty for the bare surface ($0.1e^-$) has a stronger interaction with $2\pi_x$ since it is nearer in energy and is pushed below E_F. This interaction is a typical interaction between two empty orbitals, which leads to a bonding part below E_F and therefore yields a filling of both orbitals. Therefore, the spin-up part of d_{xz} gains electrons ($+0.13$) as does that of $2\pi_x$ (0.122). The result is that globally d_{xz} (or d_{yz}) gains electrons ($+0.07$) and its associated magnetic moment decreases from 0.89 to 0.70 μB. In the same time, a spin polarization appears for $2\pi_x$ (-0.017 μB).

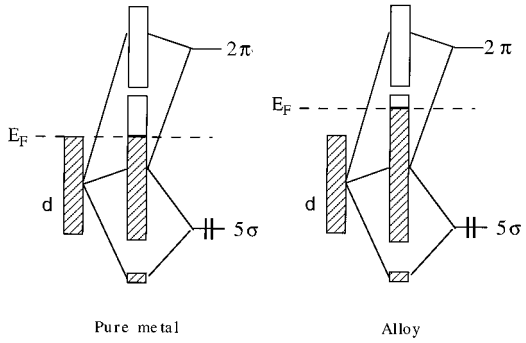

FIG. 8. Schematic diagram for the interaction between the CO molecular orbitals and the *d* band of the metal atom involved in the adsorption.

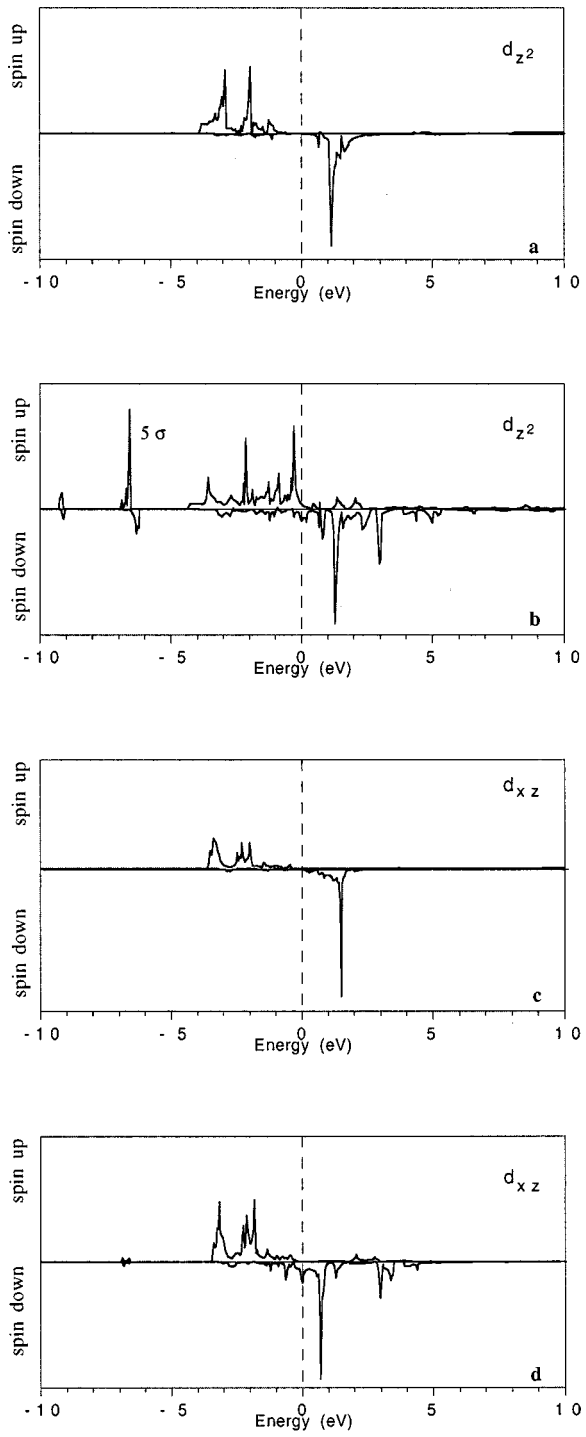

FIG. 9. DOS projected on d_{z^2} of a Mn surface atom for the bare Pd_3Mn *B* slab (a), and for the on-top CO adsorption on Mn (b).—DOS projected on d_{xz} of a Mn surface atom for the bare Pd_3Mn *B* slab (c) and for the on-top CO adsorption on Mn (d).

This detailed analysis of the orbital interactions shows the more important role of the 2π orbitals and the less important one of the 5σ orbital for the on-top adsorption of CO on Pd_3Mn compared with pure Pd. It also explains why the magnetic moment of the Mn atoms diminishes when the adsorption occurs on these atoms.

Spin-restricted calculations have been done in the case of the $Pd_3Mn(100)$ surface of type *B* with the same geometries as for the spin-unrestricted ones and with the two-layer slab.

TABLE V. CO adsorption on $Pd_3Mn(100)$ type *B* (Pd and Mn atoms in the surface): spin-restricted calculations on the two-layer slab.

	Top Pd	Top Mn	Bridge	Hollow
BE (BP)[a]	−24.1	−47.3	−35.9	−34.4
BE (PW)	−27.4	−50.6	−39.4	−38.3
C-O op	0.608	0.604	0.567	0.499
Pd-C op	0.354		0.256	0.254
Mn-C op		0.363	0.220	0.267

[a]BP: Becke 88-Perdew 86; PW=Perdew/Wang 91. See text.

The results are given in Table V. The CO adsorption energies are much stronger and the relative stability of the various adsorption sites is totally different from that obtained when spin polarization is taken into account. This time, the on-top adsorption on Mn is the most stable, then the bridge and the hollow sites are of equal stability and the top site on Pd is far less stable. The most important BE variation is for the top site on Mn. Let us compare this site for the magnetic and the nonmagnetic slabs. First, the magnetic slab itself is more stable than the nonmagnetic one by 2.9 eV. Therefore, the spin polarization induces a large stabilization. The Fermi level of the magnetic slab is 0.15 eV higher. The Mulliken population analysis gives a loss of $0.52e^-$ for 5σ in the nonmagnetic case, compared with $0.44e^-$ in the magnetic case and a gain of $0.26e^-$ for each 2π orbital, compared with $0.23e^-$. Therefore, both interactions are stronger for the nonmagnetic case, which explains the better BE and the better Mn-C op. In the same time, the d_{z^2} Mn orbital loses $0.455e^-$ instead of gaining electons as in the magnetic case and d_{xz} gains $0.362e^-$ compared with $0.066e^-$ in the magnetic case.

Let us consider the DOS projected on these orbitals (Fig. 10). The comparison of the nonmagnetic bare slab [Figs. 10(a) and 10(c)] and of the magnetic bare slab [Figs. 9(a) and 9(c)] shows the important splitting of d_{z^2} and d_{xz} due to the spin polarization. In the nonmagnetic case, the highest density of states is at the Fermi level. This is the reason why d_{z^2} can easily be pushed above E_F by interaction with 5σ and lose more electrons than in the magnetic case. This point is very important for the chemisorption strength since these depopulated states have a surface-adsorbate antibonding character. For the same reason, d_{xz} can easily be pushed below E_F by interaction with $2\pi_x$ and gain more electrons, as also does $2\pi_x$. To summarize, both 5σ and $2\pi_x$ have a more stabilizing interaction with the metal *d* bands for the nonmagnetic case than for the magnetic one because of the position of these bands closer to E_F. This explains the much larger binding energy for the nonmagnetic case.

We can conclude from this study that the adsorption of CO on an atom having a magnetic moment is less favorable than on a nonmagnetic atom and that the adsorption is associated with a decrease of this moment. This can be related with the closed shell nature of the CO fragment. For Mn the magnetic state corresponds to an almost full spin-up band and an almost empty spin-down band. This situation is clearly less favorable for the interaction with CO than the double half-filled *d* band associated with the nonmagnetic state. The half-filled band situation indeed allows to optimize the donation and back donation interactions with CO. The less favorable adsorption on a magnetic atom explains also why the bridge and hollow sites are so weakly bound on the alloy compared with pure palladium, since they both involve Mn atoms (one for the bridge and two for the hollow). To our knowledge, the relation between magnetism and molecular chemisorption has not been detailed in the literature. If the adsorption of magnetic molecules on nonmagnetic sur-

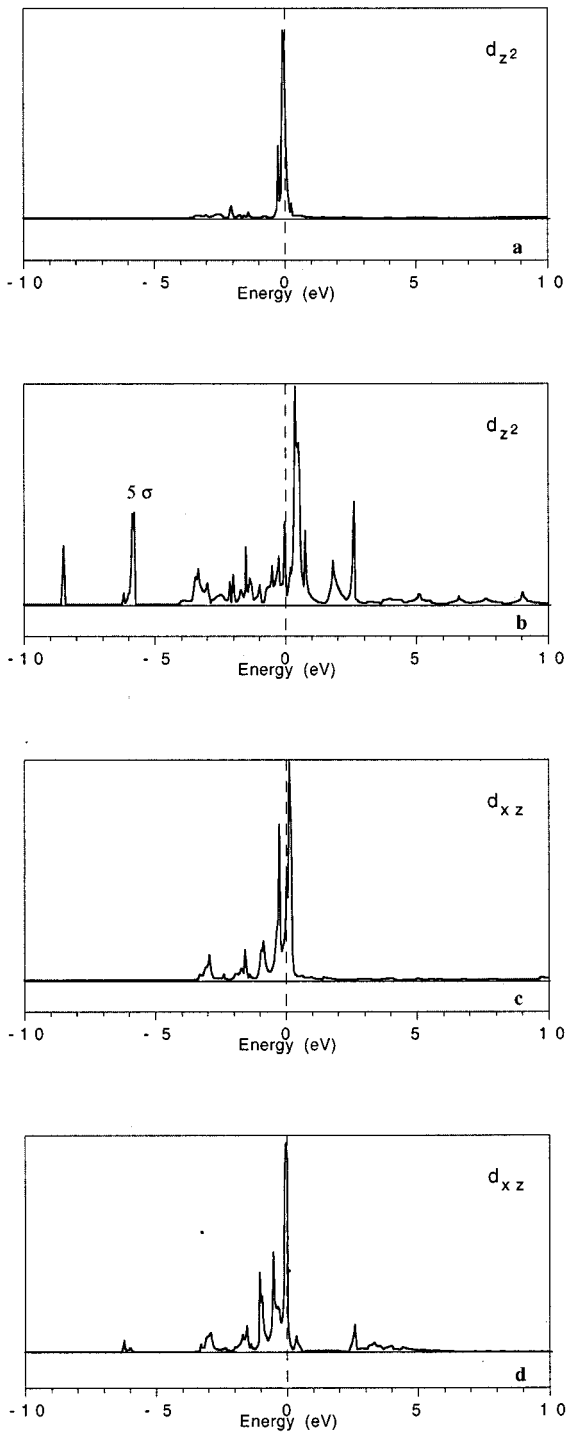

FIG. 10. Spin-restricted calculation: DOS projected on d_{z^2} of a Mn surface atom for the bare Pd_3Mn *B* slab (a), and for the on-top CO adsorption on Mn (b)—DOS projected on d_{xz} of a Mn surface atom for the bare Pd_3Mn *B* slab (c) and for the on-top CO adsorption on Mn (d).

faces has recently attracted some attention [NO on Pd, Pt (Refs. 69–71)], only a few works deal with adsorption of molecules on magnetic surfaces [N, C, O on Fe, V,[72] O_2 on Ag, Pt (Refs. 73 and 74)]. We are ourselves working on the adsorption of NO on Pd_3Mn.[75]

V. CONCLUSION

The results presented in this work are in good agreement with the experimental data. The method used, based on periodic calculations using the DFT theory at the nonlocal level, allows a good understanding of the phenomena, chemisorption strength and variation of the magnetic moments, through the analysis of the orbital interactions. The most interesting results are the following:

—On Pd(100), the most stable adsorption sites are the bridge and the hollow ones. The binding energy of the bridge site is close to the value found experimentally for the same coverage. As it was previously assumed, the main interactions involve the 5σ and $2\pi_x$ orbitals of CO (Blyholder model).

—On $Pd_3Mn(100)$ (type *A*), the relative stability of the sites is the same as that found on Pd(100), but with smaller binding energies. The 5σ donation to the metal is decreased and, in opposite, the 2π back donation is increased.

—On $Pd_3Mn(100)$ (type *B*), which can be a good representation of the real catalyst, the relative stability of the sites is changed and the most stable one is the on-top site on a Pd atom. The hollow site is this time less stable than the bridge one and the less stable site is the on-top one on a Mn atom. The best binding energy on Pd_3Mn is smaller than the best one on pure Pd, which means that globally CO is less strongly bound on the alloy, as it is observed experimentally for most alloys (no data are available for Pd_3Mn).

—Our calculations have pointed out that CO adsorption on an atom having a magnetic moment is less favorable than on a nonmagnetic atom.

—We can compare the present results with those obtained previously with the extended Hückel method (EHT) for Pd(100) and $Pd_3Mn(100)$ type *A*.[27] The conclusions are similar although the absolute values are totally different and the effects exaggerated with the semiempirical method. For instance, we observed also a diminution of the binding energy on the alloy, a diminution of the 5σ donation and an increase of the back donation. The only difference between the two methods is in the relative stability of the hollow 1 and hollow 2 sites, which is opposite. This is due to the presence of the magnetic Mn atom just below in the hollow 1 site. In fact the EHT method does not take the spin polarization into account. Likely, both methods would give different results for surfaces containing magnetic atoms like $Pd_3Mn(100)$ type *B* or $Pd_3Mn(111)$.

*Author to whom correspondence should be addressed. FAX: 33-4 72445399. Electronic address: delbecq@catalyse.univ-lyon1.fr

[1] M. T. Paffett, S. C. Gebhard, R. G. Windham, and B. E. Koel, J. Phys. Chem. **94**, 6831 (1990).
[2] C. Xu and B. E. Koel, Surf. Sci. Lett. **304**, L505 (1994).
[3] C. Xu and B. E. Koel, Surf. Sci. **327**, 38 (1995).
[4] A. F. Lee, C. J. Baddeley, M. S. Tikhov, and R. M. Lambert, Surf. Sci. **373**, 195 (1997).
[5] A. Atli, M. Abon, P. Beccat, J. C. Bertolini, and B. Tardy, Surf. Sci. **302**, 121 (1994).
[6] A. Nordermeer, G. A. Kok, and D. E. Nieuwenhuys, Surf. Sci. **172**, 349 (1986).
[7] A. Rochefort, M. Abon, P. Delichere, and J.-C. Bertolini, Surf. Sci. **294**, 43 (1993).
[8] Y. Debauge, M. Abon, J.-C. Bertolini, J. Massardier, and A. Rochefort, Appl. Surf. Sci. **90**, 15 (1995).
[9] A. Atli, M. Abon, and J. C. Bertolini, Surf. Sci. **287/288**, 110 (1993).
[10] R. Wu, Chem. Phys. Lett. **238**, 99 (1995).
[11] J. A. Rodriguez and M. Kuhn, Surf. Sci. Lett. **365**, L669 (1996).
[12] R. Wu, L. J. Chen, and N. Kioussis, Chem. Phys. Lett. **258**, 228 (1996).
[13] J. A. Rodriguez and M. Kuhn, J. Phys. Chem. **98**, 11 251 (1994).
[14] S. Pick, Chem. Phys. Lett. **239**, 84 (1995); J. Phys.: Condens. Matter **7**, 7729 (1995).
[15] R. M. Ferullo and N. J. Castellani, Langmuir **12**, 70 (1996).
[16] B. Hammer, Y. Morikawa, and J. K. Norskov, Phys. Rev. Lett. **76**, 2141 (1996).
[17] S. P. Mehandru, A. B. Anderson, and P. N. Ross, J. Catal. **100**, 210 (1986).
[18] S. Pick, J. Phys.: Condens. Matter **9**, 141 (1997).
[19] Y. T. Wong and R. Hoffmann, J. Phys. Chem. **95**, 859 (1991).
[20] S. Pick, Solid State Commun. **102**, 829 (1997).
[21] R. Ramprasad, K. M. Glassford, J. B. Adams, and R. I. Masel, Surf. Sci. **360**, 31 (1996).
[22] P. Hu, D. A. King, S. Crampin, M.-H. Lee, and M. C. Payne, Chem. Phys. Lett. **230**, 501 (1994).
[23] P. H. T. Philipsen, G. te Velde, and E. J. Baerends, Chem. Phys. Lett. **226**, 583 (1994).
[24] P. Hu, D. A. King, M.-H. Lee, and M. C. Payne, Chem. Phys. Lett. **246**, 73 (1995).
[25] A. Eichler and J. Hafner, Phys. Rev. B **57**, 10 110 (1998).
[26] F. Delbecq and P. Sautet, J. Catal. **164**, 152 (1996).
[27] F. Delbecq, B. Moraweck, and L. Verite, Surf. Sci. **396**, 156 (1998).
[28] F. Delbecq, Surf. Sci. Lett. **389**, L1131 (1997).
[29] A. El Hamdaoui, G. Bergeret, J. Massardier, M. Primet, and A. Renouprez, J. Catal. **148**, 47 (1994).
[30] J. F. Trillat, Thesis, Université Claude Bernard, Lyon, 1997; J. F. Trillat, J. Massardier, B. Moraweck, H. Praliaud, and A. Renouprez (unpublished).
[31] G. te Velde and E. J. Baerends, Phys. Rev. B **44**, 7888 (1991); J. Comput. Phys. **99**, 84 (1992).
[32] A. D. Becke, Phys. Rev. A **38**, 3098 (1988); J. P. Perdew, Phys. Rev. B **33**, 8822 (1986).
[33] J. P. Perdew and Y. Wang, Phys. Rev. B **45**, 13 244 (1992).
[34] F. Delbecq, L. Verite, and P. Sautet, Chem. Mater. **9**, 3072 (1997).
[35] C. L. Fu, A. J. Freeman, and T. Oguchi, Phys. Rev. Lett. **54**, 2700 (1985).
[36] A. J. Freeman and R. Wu, J. Magn. Magn. Mater. **100**, 497 (1991).
[37] J. Mathon, Rep. Prog. Phys. **51**, 1 (1988).
[38] S. Blügel, M. Weinert, and P. H. Dederichs, Phys. Rev. Lett. **60**, 1077 (1988).

[39] I. Turek, S. Blügel, and J. Kudrnovsky, Phys. Rev. B **57**, R11 065 (1998).
[40] R. Wu, C. Li, and A. J. Freeman, J. Magn. Magn. Mater. **99**, 71 (1991).
[41] M. J. Zhu, D. M. Bylander, and L. Kleinman, Phys. Rev. B **42**, 2874 (1990).
[42] J. G. Gay, J. R. Smith, F. J. Arlinghaus, and T. W. Capehart, Phys. Rev. B **23**, 1559 (1981).
[43] P. Nordlander, S. Holloway, and J. K. Norskov, Surf. Sci. **136**, 59 (1984).
[44] J. Rogozik, J. Küppers, and V. Dose, Surf. Sci. **148**, L653 (1984).
[45] P. D. Johnson and S. L. Hulbert, Phys. Rev. B **35**, 9427 (1987).
[46] V. Frorentini, M. Methfessel, and M. Sheffler, Phys. Rev. Lett. **71**, 1051 (1993).
[47] D. Rodic, P. J. Ahlzen, Y. Anderssons, R. Tellgren, and F. Bouree-Vigneron, Solid State Commun. **78**, 767 (1991).
[48] J. W. Cable, E. O. Wollan, W. C. Koehler, and H. R. Child, Phys. Rev. **128**, 2118 (1962).
[49] J. A. Rodriguez and D. W. Goodman, Science **257**, 897 (1992).
[50] R. Wu and A. J. Freeman, Phys. Rev. B **52**, 12 419 (1995).
[51] G. K. Wertheim and J. E. Rowe, Science **260**, 1527 (1993).
[52] R. Wu, Chem. Phys. Lett. **238**, 99 (1995).
[53] M. Wuttig, B. Feldmann, and T. Flores, Surf. Sci. **331**, 659 (1995).
[54] J. C. Tracy and P. W. Palmberg, J. Chem. Phys. **51**, 4852 (1969).
[55] R. J. Behm, K. Christmann, G. Ertl, M. A. van Hove, P. A. Thiel, and W. H. Weinberg, Surf. Sci. **88**, L59 (1979).
[56] R. J. Behm, K. Christmann, G. Ertl, and M. A. van Hove, J. Chem. Phys. **73**, 2984 (1980).
[57] A. Ortega, F. M. Hoffman, and A. M. Bradshaw, Surf. Sci. **119**, 79 (1982).
[58] P. Uvdal, P. A. Karlsson, C. Nyberg, S. Anderson, and N. V. Richardson, Surf. Sci. **202**, 167 (1988).
[59] J. Szanyi, W. K. Kuhn, and D. W. Goodman, J. Vac. Sci. Technol. A **11**, 1969 (1993).
[60] S. Ishi, Y. Ohno, and B. Viswanathan, Surf. Sci. **161**, 349 (1985).
[61] H-K Hu and J. W. Rabalais, Surf. Sci. **107**, 376 (1981).
[62] I. Toyoshima and G. A. Somorjai, Catal. Rev. Sci. Eng. **19**, 105 (1979).
[63] J. C. Tracy and P. W. Palmberg, Surf. Sci. **14**, 274 (1969).
[64] B. E. Nieuwenhuys, Surf. Sci. **105**, 505 (1981).
[65] G. Blyholder, J. Phys. Chem. **68**, 2772 (1964).
[66] A. Sandell, O. Björneholm, J. N. Andersen, A. Nilson, E. O. F. Zdansky, B. Hernnäs, U. O. Karlsson, R. Nyholm, and N. Martensson, J. Phys.: Condens. Matter **6**, 10 659 (1994).
[67] S. P. Mehandru, A. B. Anderson, and P. N. Ross, J. Catal. **100**, 210 (1986).
[68] G. Kresse and J. Hafner, Phys. Rev. B **47**, 558 (1993); G. Kresse and J. Furthüller, Comput. Mater. Sci. **6**, 15 (1996).
[69] K. C. Hass, M.-H. Tsai, and R. V. Kasowski, Phys. Rev. B **53**, 44 (1996).
[70] B. Hammer and J. K. Norskov, Phys. Rev. Lett. **79**, 4441 (1997).
[71] Q. Ge and D. A. King, Chem. Phys. Lett. **285**, 15 (1998).
[72] S. Pick and H. Dreysse, Surf. Sci. **394**, 192 (1997).
[73] P. A. Gravil, D. M. Bird, and J. A. White, Phys. Rev. Lett. **77**, 3933 (1996).
[74] A. Eichler and J. Hafner, Phys. Rev. Lett. **79**, 4481 (1997).
[75] F. Delberg and P. Sautet, Chem. Phys. Lett. (to be published).